



## Mechanical and thermal characterisation of AlSi10Mg SLM block support structures

Martin Leary <sup>a, b, c,\*</sup>, Tobias Maconachie <sup>a, b, c</sup>, Avik Sarker <sup>a</sup>, Omar Faruque <sup>b, c</sup>, Milan Brandt <sup>a</sup>



<sup>a</sup> RMIT Centre for Additive Manufacture, RMIT University, Melbourne, Australia

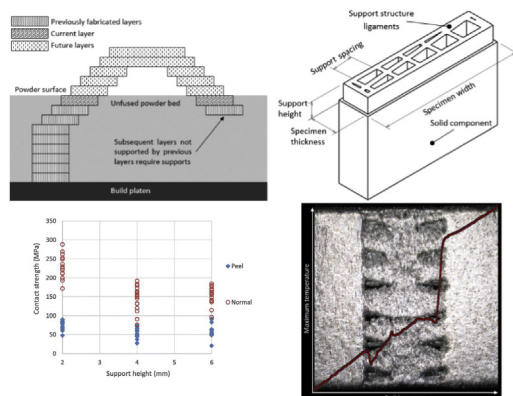
<sup>b</sup> Ford Motor Company, Research Innovation Centre (RIC), Dearborn, MI, USA

<sup>c</sup> ARC Training Centre for Lightweight Automotive Structures (ATLAS), Australian Research Council Grant IC160100032, Australia

### HIGHLIGHTS

- Analysis of the mechanical strength and thermal properties of AlSi10Mg block support structures fabricated by SLM.
- The peel strength of a support structure is significantly less than its tensile strength.
- The strength of a support structure is inversely proportional to its height.
- Reducing support spacing increases heat transfer capability.

### GRAPHICAL ABSTRACT



### ARTICLE INFO

#### Article history:

Received 11 April 2019

Received in revised form

15 August 2019

Accepted 19 August 2019

Available online 19 August 2019

#### Keywords:

Support structures

Heat transfer

Mechanical properties

Manufacturability

Powder bed fusion

### ABSTRACT

Selective Laser Melting (SLM) is an Additive Manufacturing (AM) process based on the local fusion of powdered metal. SLM requires support structures that enable heat transfer and structural support during fabrication while being frangible to enable removal. Despite the criticality of support structures, very little quantitative data exists to characterise their behaviour. AlSi10Mg is an important SLM alloy which is particularly appropriate for laser applications due to its ease of processing. Block support structures are the most versatile of the commercially implemented support structure designs. This research presents an experimental study of the mechanical strength and numerical analysis of the thermal behaviour during SLM fabrication of AlSi10Mg block support structures. It was found that: support structure peel strength is significantly lower than normal strength due to fundamentally different failure mechanisms; support strength is influenced by height; and, reduced support spacing increases heat transfer and load bearing capability. Design equations were generated to enable prediction of the strength of a given support structure. This previously unavailable data allows AM designers to unambiguously specify support structures that are optimal for a specific design scenario. Furthermore, these insights potentially allow the redesign of block support structures such that response is independent of geometry.

© 2019 Published by Elsevier Ltd. This is an open access article under the CC BY-NC-ND license (<http://creativecommons.org/licenses/by-nc-nd/4.0/>).

\* Corresponding author at: RMIT Centre for Additive Manufacture, RMIT University, Melbourne, Australia.

E-mail address: [martin.leary@rmit.edu.au](mailto:martin.leary@rmit.edu.au) (M. Leary).

## 1. Introduction

Additive manufacturing (AM) enables the fabrication of components with a complexity that cannot be achieved by traditional subtractive manufacturing [1]. Selective Laser Melting (SLM) is a powder-bed fusion AM technology in which three-dimensional components are produced from CAD data by fusion of metallic powder layer-by-layer using a laser energy source. This fusion is a complex thermo-mechanical process whereby a transient melt pool is established within a highly non-linear material that is thermally and geometrically transient [2]. This transient behaviour during solidification significantly affects the associated geometric and mechanical properties of components fabricated by this process [3]. During SLM manufacture components experience large thermal gradients that induce residual stresses [4]. These stresses are undesirable as they may compromise structural integrity and can lead to distortion of fabricated geometries [5].

Support structures are invaluable for AM as they serve multiple technical functions and increase the range of manufacturable geometries. Support structures can be used to actively increase heat transfer to manage residual stresses and local temperature fields [6] which is particularly important for SLM. Where thermal stresses cannot be eliminated, support structures can also physically resist component distortion. Acutely overhanging features can compromised build quality or even cause catastrophic failure of fabricated components without the use of support structures [7]. Support structures also provide physical support to slender geometries [8] and are used to offset the manufactured component from the platen to aid in component removal. A variety of support structure designs have been implemented in commercial AM software or proposed in the literature. The most versatile and commonly applied of these are referred to as "block" support structures, and as such are the focus of this study.

Although they provide technical advantages for AM design, the use of support structures can significantly increase manufacturing time and material consumption, and therefore the cost of manufacture. Support structures can also increase the cost of post-processing and their removal can negatively affect surface quality [1]. Support structures therefore present competing design objectives: they must be sufficiently strong to provide necessary support while being adequately frangible to allow post-manufacture removal. For these reasons the optimisation of support structure design is important for the commercial application of SLM AM. However, despite the necessity of robust support structures, there exists little research available on support structure design and optimisation [9].

Due the importance of titanium for aerospace and biomedical applications [10] available literature on SLM support structure design is primarily focussed on titanium alloys [8,11]. However, aluminium alloys are receiving increased research attention for AM [12] as they provide technical and economic opportunities including good strength-to-weight and cost-to-strength ratios [13], high thermal diffusivity [14] and excellent corrosion resistance [15]. Yet this increased attention has not been complemented by formal research on support structure design for SLM aluminium alloys. Specifically, there is an absence of prescriptive design for AM (DFAM) rules for the specification of effective support structures – an omission that restricts the commercial application of aluminium AM. The aluminium alloy used in this work, AlSi10Mg, is a commonly used AM alloy due to its excellent properties and ease of processing for laser applications [16].

In response to this identified deficiency, this research contributes the following:

- Existing methods of support structure design are reviewed, including commercially-implemented support structures as well as those proposed in the literature.

- A full-factorial Design of Experiments (DOE) is generated for block-type support structures manufactured by SLM with AlSi10Mg for selected geometric control factors.
- Manufactured specimens are scanned using micro computed tomography ( $\mu$ CT) to allow qualitative and quantitative characterisation of the as-manufactured support structure geometry.
- The mechanical properties of these support structures are quantified for peel and normal loading scenarios.
- Numerical thermal analysis is applied to provide insight into the thermal behaviour of support structures during SLM fabrication.

To enhance the commercial application of aluminium AM, prescriptive DFAM rules are defined from this novel research to allow systematic specification of support structure parameters to achieve a specific mechanical response.

## 2. Support structure design

Support structures provide several technical functions, including: structural support; increased heat transfer; frangibility for ease of part removal; and, physical resistance to bulk structural deformation.

During the SLM process, previously fabricated material provides structural support for subsequent layers (Fig. 1, A). However, when the current layer overhangs the previous layer (Fig. 1, B) the unfused powder bed provides the only structural support to the overhanging regions which may be inadequate. The critical inclination angle of an unsupported surface below which manufactured geometry is likely to be compromised is dependent on material and machine process parameters [17], but is usually approximated as 45° [18]. Isolated component features (Fig. 1, C) will be brushed away by the recoater blades and are not directly manufacturable. Support structures overcome these challenges by providing physical support to overhanging and isolated features.

Support structures affect local temperature during fabrication by providing additional pathways for thermal conduction. Residual stresses resulting from the extreme thermal gradients within components during manufacture may cause deformation of fabricated geometries. The inclination angle of downward-facing surfaces also has implications for thermal distortion as the temperature of these surfaces increases as inclination angle decreases (Fig. 2). Support structures can resist this deformation [19] both by increasing heat transfer and by physically grounding the fabricated geometry to the build platen.

Frangibility is defined as 'the property which allows an object to break, distort, or yield at a certain impact load while absorbing minimal energy' [20]. AM support structures should be adequately frangible to allow easy removal and minimise post-processing difficulty. Frangibility of SLM support structures is improved by the inclusion of teeth (Fig. 3) which encourage fracture at the component and build platen interfaces.

Support structures are commonly used to provide a frangible interface to offset the manufactured component from the build platen. This interface protects the component and platen from damage and reduces post-processing time [21].

### 2.1. Specific support structures

A range of support structure designs have been implemented in commercial software (Fig. 4) or proposed in academic literature (Fig. 5). These support structures have various technical attributes that are appropriate for specific applications. For example, line supports are compatible for thin sections, whereas web supports are preferable for circular surfaces.

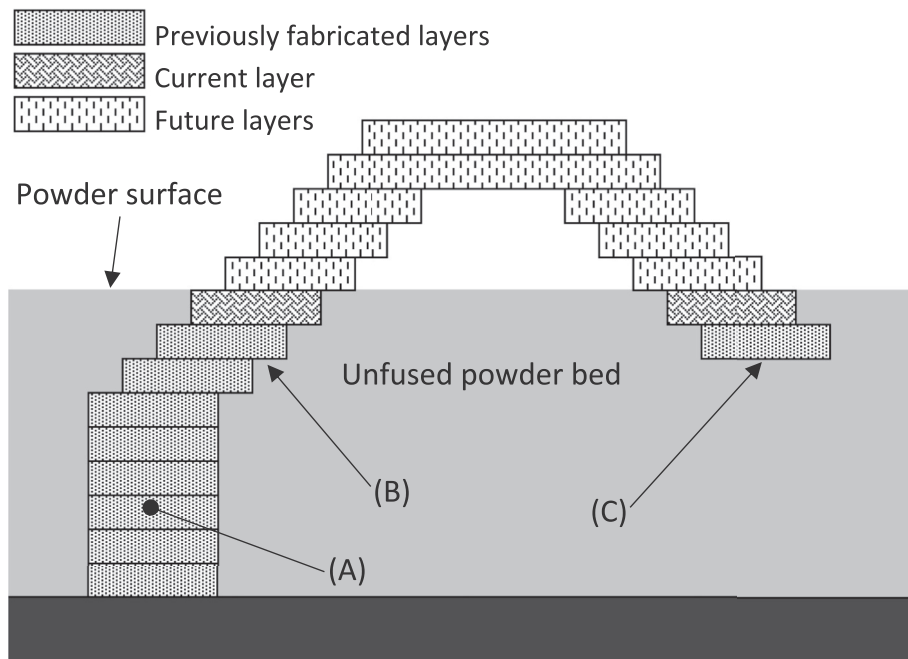


**Fig. 1.** Schematic representation of the support provided by previous layers during fabrication. Previous layers fully support subsequent layers where no overhanging features exist (A). When subsequent layers overhang previous layers the unfused powder bed provides partial support (B), however a critical inclination exists beyond which support structures are required. Isolated features (C) require support structures to ground them.

Block supports are the most versatile and generic of the commercially implemented support structure designs as they are easily defined and provide evenly-distributed support over a large area. As a result, they are one of the most commonly applied support structure design, particularly for providing an interface between fabricated components and the build platen. For this reason, block support structures are the focus of this research.

## 2.2. Existing literature on support structure design

Within the literature of AM, some explore support structures in general terms. For example, Jiang et al. provide a comprehensive review of support structures for AM and provide a taxonomy for AM support structure design, including the distinction of approaches that modify the nominal AM geometry to minimise the necessity of support structures [9]. Others offer specific means of improving or minimising the need for support structures.

Bobbio et al. [11] investigated the strength of support structures in Ti64 fabricated by SLM. They found the effective structural strength, defined as the total force the structure withstood divided

by the total cross-sectional area, to be 14–32% of fully dense material. This reduced strength is explained by stress concentrations at the support structure-solid material interfaces.

Calignano used the Taguchi method to determine the condition most suitable for reducing deformation of parts while allowing easy removal of support structures for most geometries when manufacturing using SLM [7]. 0.5 mm hatch spacing was found to be optimum for aluminium alloys, and 0.75 mm for titanium. 0.43 mm teeth height and 0.1 mm teeth base interval were optimal regardless of material. Support structure removal was qualitatively characterised according to the ease of support structure removal.

Cloots et al. propose a specific component segmentation strategy whereby a component is divided into critical areas according to the presence of surrounding material which may behave as a heat sink and a specific laser scanning method is applied for each of these depending on their needs [21]. Modulating energy input generally reduces support requirements in these areas and can allow manufacture of overhanging features with an inclination angle  $<35^\circ$ .

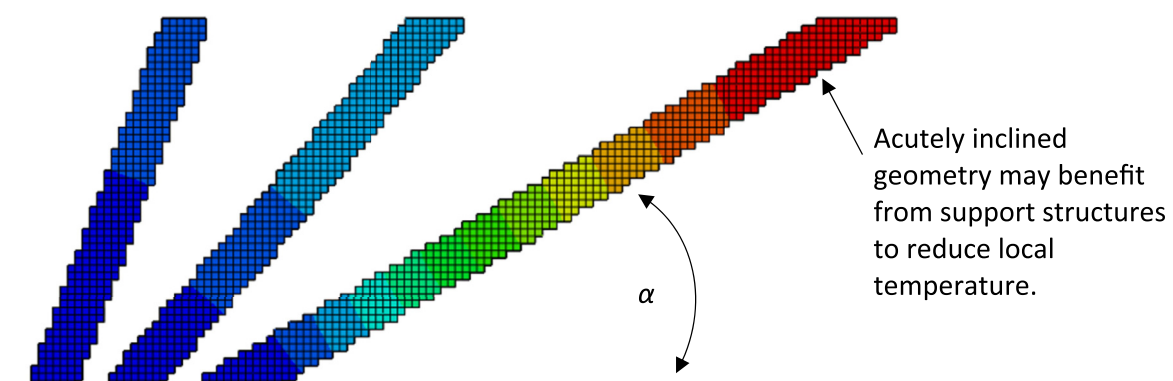


**Fig. 2.** Schematic representation of the increase in temperature associated with a reduced inclination angle,  $\alpha$ . Support structures may be beneficial to ground thermal loads.

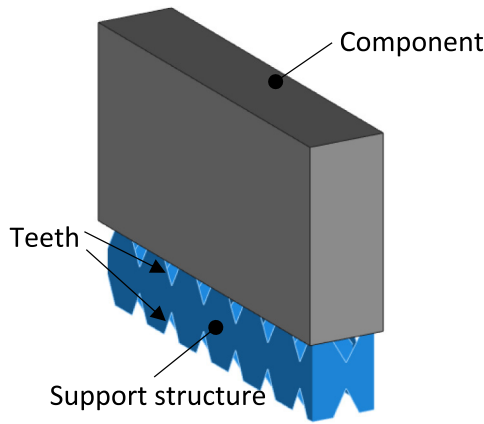


**Fig. 3.** Commercially implemented block-type support structure (blue). Frangibility is increased by the inclusion of triangular gaps (teeth) that also allow unmelted powder to escape.

Hussein et al. found that for lattice support structures the type of structure, volume fraction and cell size are the main factors influencing manufacturability [8]. Suitability of these structures

was measured by material and build-time reduction and deflection of supported areas.

A new approach to improve support structure design which optimises part build orientation and support cellular structure is proposed by Strano et al. [23]. An optimisation algorithm based on pure mathematical implicit functions is used to generate functionally-graded cellular support structures. This method was found to reduce material waste by up to 45%.

A support structure generation tool based on laser scan patterns and thermo-mechanical simulation tools for SLM has been developed by Zeng [25]. He found the effective thermal properties of support structures to be a function of their geometry, anisotropy and constituent independent thermal properties. Results of this method were found to adequately match accepted conventional models.

### 3. Experimental method

Despite extensive review, no literature was found that provides design quality insight into the response of AlSi10Mg block support structures for SLM. In response to this deficiency an experimental research program is proposed to characterise the effect of block

Type	3D view	Plan view	Type	3D view	Plan view
Block		(A)	Contour		
Line		(B)	Gusset		
Point			Volume		
Web		(C)	Cones		

**Fig. 4.** Commercially implemented support structure designs which are differentiated by the arrangement of their ligaments. The internal structure of block supports (A) are rotated by an angle ( $5^\circ$  by default) so they are not aligned with the build platen to better fill the required space regardless of dimensions and to avoid intersecting the recoater blade at a single location. Red outlines (B) represent the supported surface. Support structures are usually generated linearly but can also be generated rotationally (C). Not all support structures require attachment to a parallel underlying surface — gusset supports (D) allow attachment to a perpendicular surface. These support structures were generated using commercial AM pre-processing software [22]. (For interpretation of the references to colour in this figure legend, the reader is referred to the web version of this article.)

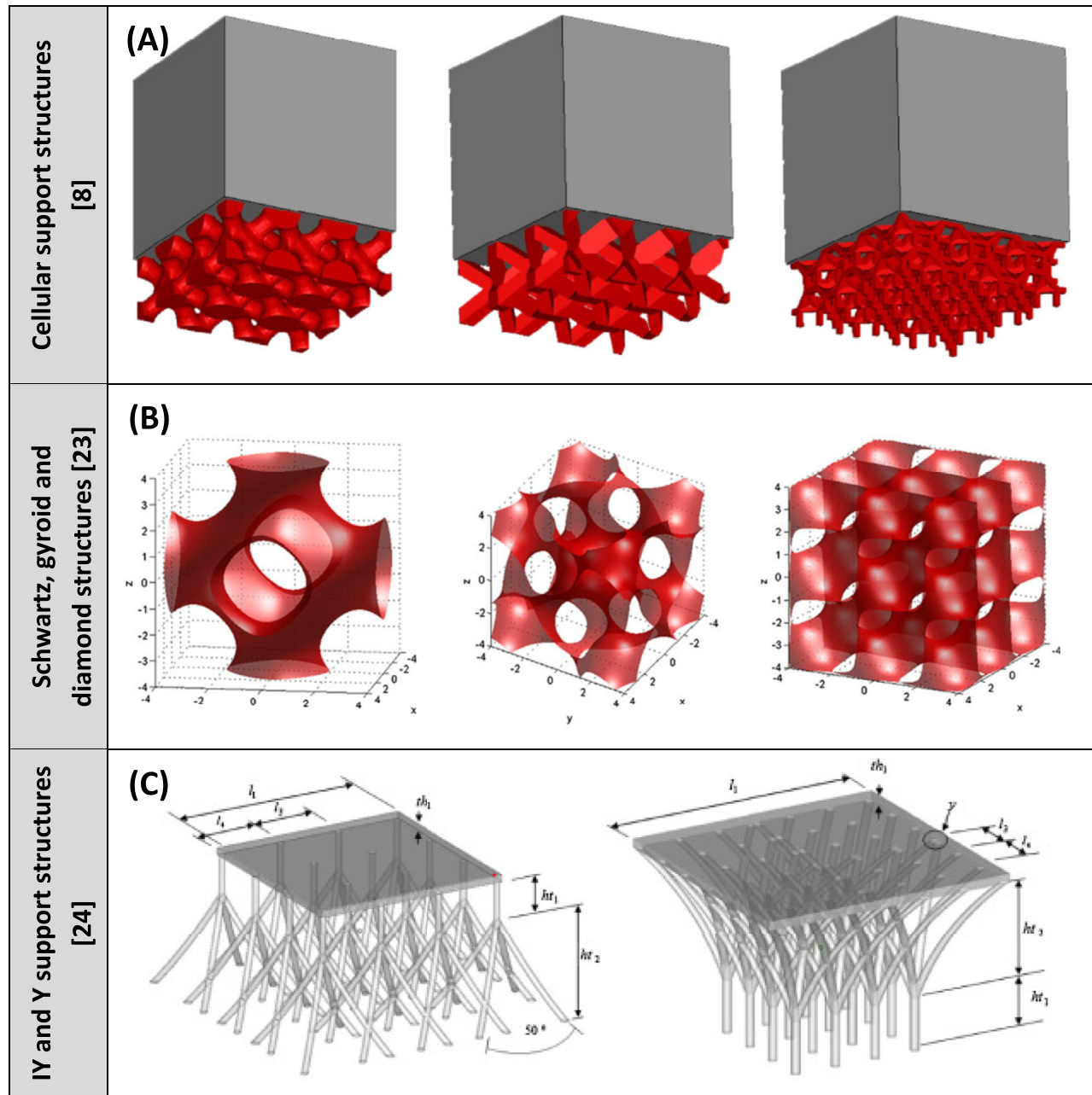


**Fig. 5.** Novel support structure designs proposed for SLM. To reduce manufacturing time and cost through improved material and energy consumption, Hussein et al. [8] used lattice structures with very low volume fraction as supports (A). Strano et al. [23] used pure mathematical 3D implicit functions to generate support structure geometries (B). Gan and Wong [24] prioritised maintaining levelness in AM and developed support structures consisting of uniformly-spaced vertical struts to achieve this.

support structure geometry parameters on the following attributes:

- As-manufactured specimen geometry.
- Mechanical response for peel and normal loading scenarios.
- Thermal behaviour during fabrication.

A full factorial design of experiments method was implemented to generate predictive tools for improved support structure design.

### 3.1. Control factors

The defining geometric features of a block support structure are: the arrangement of its ligaments, referred to as 'type' (Fig. 4); the vertical distance bridged by the support structure; and, the

associated cross-sectional area. Cross-sectional area is a function of the hatch spacing (distance between laser scan paths) defined during support generation.

Block supports are the most common and versatile of the standard support structure designs (Section 2.1) and are the focus of this research. The control factors used to define support structure geometry were support height and spacing (Fig. 6).

Normal strength is a standard method of quantifying the strength of porous [26] and AM structures [11]. However, this method fails to capture a key loading condition experienced by components during SLM fabrication. Deformation of fabricated geometry can occur during SLM where it will 'peel' away from the build platen (Fig. 7) due to residual stresses that arise during cooling [27].

To provide a thorough characterisation of support structure mechanical response, support structures were tested under two

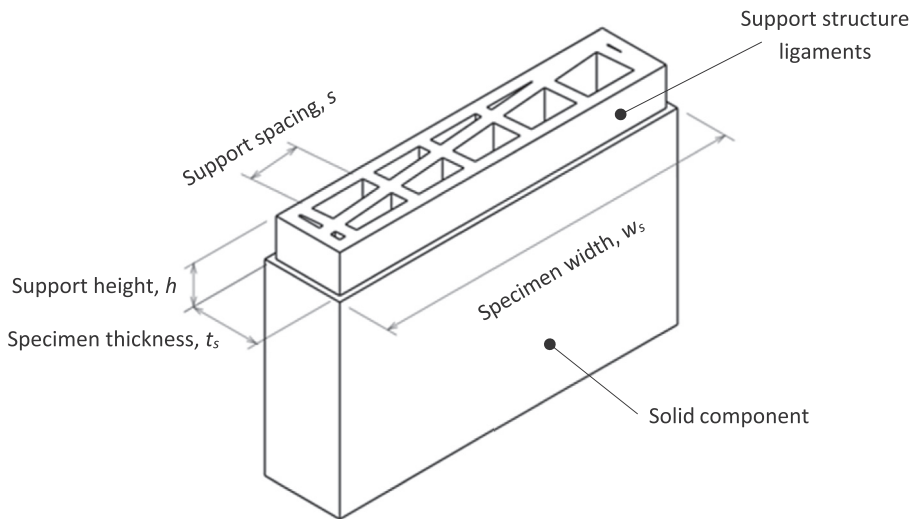


**Fig. 6.** Schematic representation of specimen geometry, including support height and spacing, and specimen width and thickness.

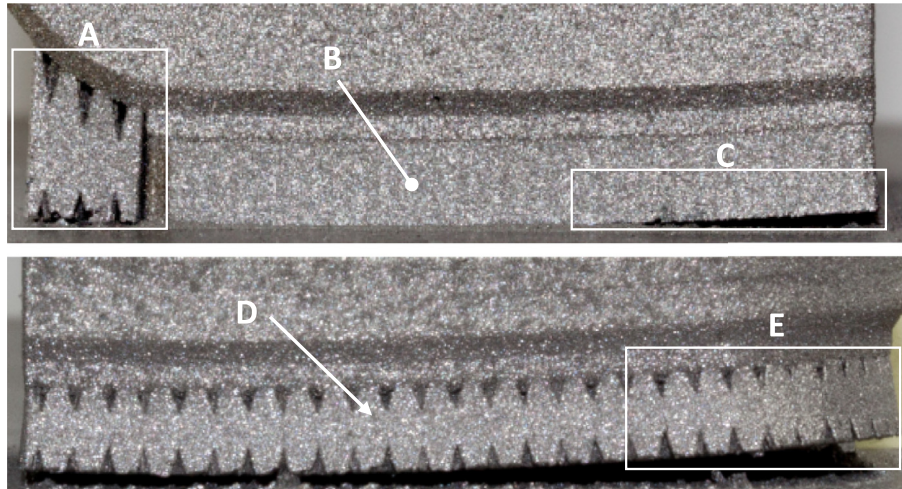


**Fig. 7.** Sample components which have detached from the platen during manufacture. Both *block* (A) and *volume* (B) type supports have failed by peel, especially at edges (C). *Block* support (D) which has entirely detached from platen, most significantly at outer edge (E).

unique loading conditions<sup>1</sup> – normal loads, as described above, and peel loads which were produced by an external load with line of action coincident to the edge of the support structure (Fig. 8).

### 3.2. Characterisation of support structure strength

The load-carrying capacity of a support structure can be quantified by the peak load ( $P_{max}$ ) grounded at failure. This capacity can be represented as the strength associated with either the supported area or contact area.

Supported area strength ( $\sigma_s$ , Eq. (1)) is associated with the supported area ( $A_s = W_s t_s$ , Fig. 6). This measure is useful for practicing engineers who intend to specify a support strength for a given supported area.

Contact strength ( $\sigma_c$ , Eq. (2)) is associated with the minimum cross-sectional area ( $A_c$ ) of the support structure. This measure provides insight into the fundamental mechanical response of

the proposed support structures and more accurately describes true structural strength. Contact area was measured from µCT data of as-manufactured geometry, and due to the presence of teeth, occurs in the region of the solid material-support structure interface.

$$\sigma_s = \frac{P_{max}}{A_s} = \frac{P_{max}}{w_s t_s} \quad (1)$$

$$\sigma_c = \frac{P_{max}}{A_c} \quad (2)$$

### 3.3. Design of experiments

Control factors used to characterise the support structure mechanical response include load type, support height and support spacing. To allow characterisation of a non-linear response, three control factor levels were selected for support height (2 mm, 4 mm and 6 mm), and four levels of support spacing were selected (0.75 mm, 1 mm, 1.25 mm and 1.5 mm). Test specimen geometries were designed according to these control factors (Fig. 8). Diamond-

<sup>1</sup> Loads generated using a 5569A Instron with a 50kN load cell with cross-head velocity of 0.5 mm/min.

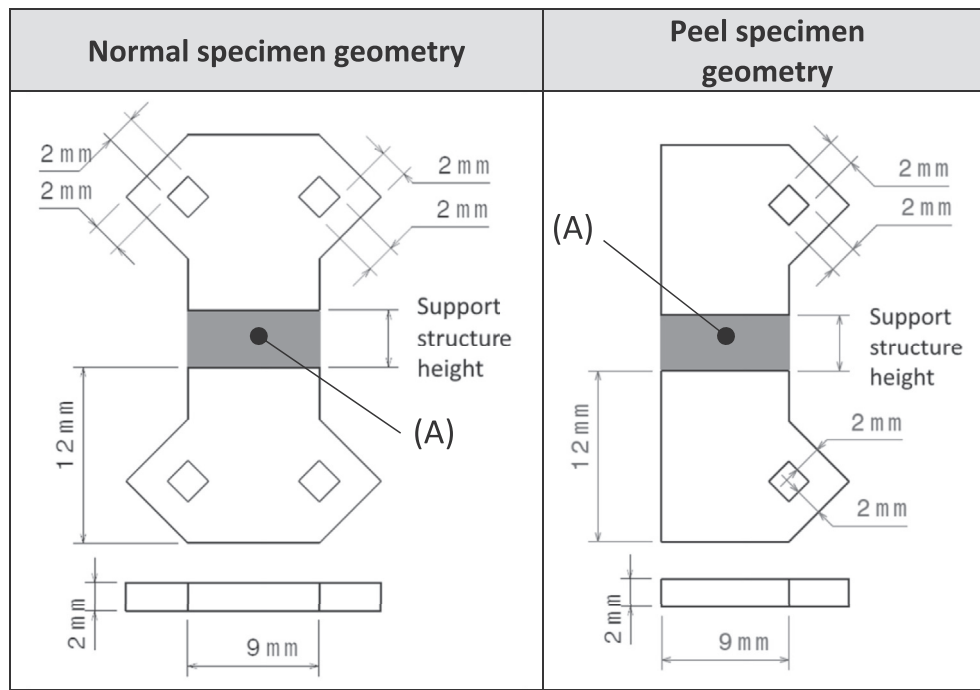


**Fig. 8.** Specimen geometry. Grey sections (A) represent support structures, the height of which varies with permutation.

shaped holes (Fig. 8, B) were included for attachment of specimens to test rig. Holes were designed with this shape for improved manufacturability – 45° is known to be the minimum reliable angle from horizontal at which components can be fabricated without requiring support [18]. Normal specimens were loaded symmetrically, whereas peel specimens were excentrically loaded (Fig. 8).

#### 3.4. Specimen manufacture

Specimens were manufactured using a 400 W dual laser powder bed SLM system<sup>2</sup> (Table 1) using AlSi10Mg powder (Table 2, Fig. 9).

#### 3.5. Numerical thermal analysis

While in-situ monitoring of the SLM process is receiving research attention due to its importance for optimisation and certification of the manufacturing process [28], in-processing monitoring is challenging for commercial systems [30] and industrial process optimisation is typically achieved by empirical observations of fabricated test coupon components [29].

However, as heat transfer characteristics are vital to the technical performance of support structures, the thermal behaviour of the support structures during the SLM fabrication process was numerically modelled to provide insight into their heat dissipation capacity. Model geometry was generated from µCT data of as-fabricated specimens. Only the behaviour of the support structure region of the models was of interest, so to reduce computation time truncated models which included the support region and small sections of solid material either side were generated (Fig. 10).

The model was meshed with linear DC3D8 diffusive heat transfer elements that were incrementally added to the model in layers to replicate the layer-wise AM fabrication method. For each step of the analysis a layer of the model was added, and energy

proportionate to the volume of the layer, the volumetric energy density, the laser power and the layer heating time was applied. Conduction between the model's layers and the build platen were the only heat transfer modes simulated. The material and processing parameters used in the thermal simulation are detailed in Table 3.

## 4. Results

The results of physical testing provide insight into the mechanical response of block support structures, and the results of thermal simulations are representative of their thermal behaviour during fabrication.

#### 4.1. As-manufactured geometry

Specimens were scanned using a Bruker Skyscan 1275 Micro CT for characterisation of the support structure as-manufactured geometry. The intended geometry, as generated in data preparation software, is compared with µCT images of the as-manufactured geometry (Fig. 11). This ideal geometry has no thickness and is essentially represented by a linear tool path, whereas the thickness of the as-manufactured geometry is related to the AM hardware, materials and associated process parameters. Although the as-manufactured geometry generally conforms to the ideal geometry, it is not perfectly formed due to the layer-wise fabrication of the PBF architecture and the complexity of melt pool behaviour during solidification (Fig. 11).

A custom script was developed to analyse µCT data to quantify the proportion of material at each cross-section through the height of the support structure (Fig. 12). This analysis provides insight into the variation of as-fabricated support geometry as a function of specimen height and support spacing and enables identification of the minimum cross-sectional area for calculation of contact stress (Section 3.2). The qualitative proportions of support structure cross-section are independent of the support height and spacing;

<sup>2</sup> Selective Laser Melting system: SLM Solutions SLM 500

**Table 1**  
SLM process parameters.

SLM parameter	Symbol	Solid section	Support
Laser power (W)	P	370	275
Laser beam diameter ( $\mu\text{m}$ )	D	90	90
Laser speed (mm/s)	V	1135	1100
Linear heat input <sup>a</sup> (J/mm)	Q	0.326	0.25
Laser energy density <sup>b</sup> ( $\text{MJ/m}^2$ )	U	4.61	3.54
Layer thickness ( $\mu\text{m}$ )	—	30	60
Hatch space (mm)	—	0.17	NA
Hatch rotation ( $^\circ$ )	—	67	NA

$$^a Q = \frac{P}{DV}$$

$$^b U = \frac{PV}{D^2}$$

i.e. the minimum cross-sectional area consistently occurs at the solid structure interface, and area increases linearly to a constant value at the teeth apex. Quantitatively, the minimum cross-section area of the support structures is larger for the 2 mm support structure height than for the other scenarios. As expected, cross-sectional area tends to increase with reduced spacing. These observations are consistent with the observed mechanical response reported in the following section (Fig. 16).

#### 4.2. Mechanical testing

The influence of load type on mechanical response was clear from the typically observed behaviour (Fig. 13). For normally-loaded specimens, as displacement increases, load increases monotonically and enters a linear region; brittle failure then occurs without warning resulting in catastrophic collapse (Fig. 13, A). The initial deformation behaviour of peel-loaded specimens matches that observed for normally-loaded specimens; however, as the initial fracture load is approached, the linear loading response is interrupted by non-linear reduction in observed load (Fig. 13, B). Fracture occurs without warning; however, this fracture is not catastrophic and is arrested at some reduced load. Subsequent load-displacement response is approximately linear until successive fracture occurs. This behaviour repeats until complete failure of the support structure (Fig. 13, C). This observed fracture sequence is coincident with the progressive failure of individual support ligaments. For normal-loading, all ligaments fail concurrently, whereas the failure of ligaments within peel specimens occurs progressively from the initial failure of the ligament that is coincident with the peel load and is progressively followed by the failure of neighbouring ligaments (Fig. 14).

When peak load was reached, despite their relatively ductile material, specimens exhibited behaviour that appears to be macroscopically brittle. However, when the fracture surface of failed specimens was examined using SEM (Fig. 15), the surface was porous, indicating locally ductile failure at the micro scale [31].

From this observed behaviour it can be inferred that stochastic

variability in ligament strength is relevant to predictions of the bulk mechanical response of SLM support structures; and that loading type influences the observed ligament fracture. To provide quantitative insight, the support and contact strengths (Section 3.2) are presented as functions of load type, support height and support spacing (Fig. 16).

The observed strength for supported area and contact area are consistently greater for normally-loaded specimens than for peel-loaded specimens. This outcome is consistent with observed specimen failure behaviour modes. Normal loads are distributed across the entire structure, thereby activating resistance from all ligaments within the support structure. Conversely, the peak stresses observed for peel loads are concentrated within specific ligaments only, thereby resulting in a weak-link failure mode with lower observed failure strength.

The experimental data suggests that strength is influenced by support height; specifically, a larger strength is typically observed for 2 mm height support structures. This observation is concurrent with the observed variation in cross-sectional area (Fig. 12), whereby 2 mm height specimens had the greatest minimum cross-sectional area, resulting in a larger reported supported area strength (Section 4.2). Interestingly, this observation is equally true for contact area strength (which is based on the observed minimum cross-sectional area), implying that the stress-concentration effect of 2 mm support structures is reduced in comparison with other support structure heights. This observation is highly relevant for the designers of support structure generation tools, as it implies that the performance of current methods of support structure generation are functionally dependant on the associated support geometry. In contrast, there appears to be relatively little influence of support spacing on the observed strength, especially for contact area strength, which is intended to account for variation in support structure cross-sectional area (Fig. 12).

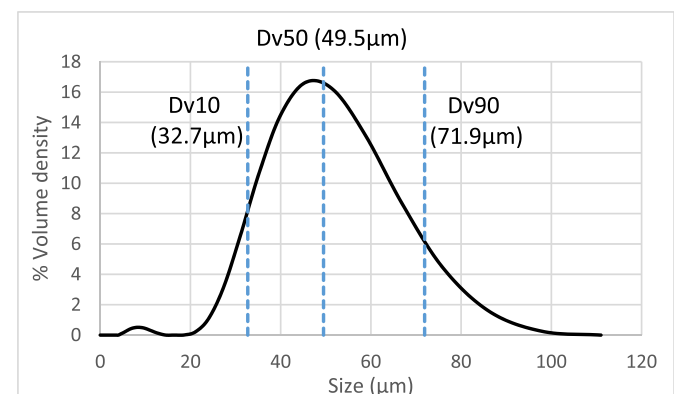


**Fig. 9.** Distribution of powder particle size by volume acquired by laser diffraction.

**Table 2**  
Chemical composition of AISI10Mg acquired by spectrographic analysis.

Element	Percent composition	Element	Percent composition
Aluminium	Balance	Titanium	0.01
Silicon	10.2	Strontium	<0.001
Copper	<0.01	Zirconium	<0.005
Iron	0.19	Vanadium	0.005
Magnesium	0.34	Silver	<0.005
Zinc	0.01	Carbon	<0.005
Chromium	0.01	Nitrogen	0.002
Nickel	0.01	Oxygen	0.12
Manganese	<0.01		

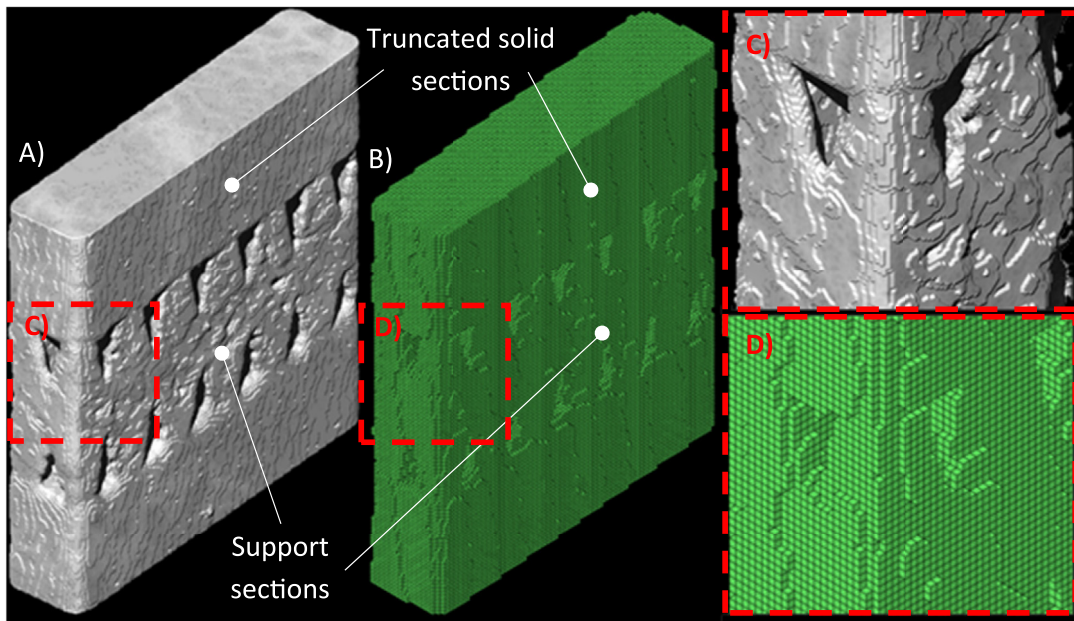


**Fig. 10.** Stereolithographic representation of  $\mu$ CT data (A) and FE model generated from hexahedral elements (B). Inspection of model surfaces show complex surface morphology is simplified in stereolithographic form (C) which is voxelised in conversion to hexahedral elements (D).

The contact strength of the support structures was found to range between 37 and 67% of the strength of the bulk material, which is comparable with previously reported results [11]. However, the supported area strength was significantly lower (8–25%), an observation that highlights the significant effect of local support structure geometry on mechanical response.

Analysis of variance (ANOVA) was performed for both supported area and contact strengths and normal and peel loads (Appendix 1, Tables 4–7). Assuming a significance level of 5%, all control factors were found to be significant in determining the associated support structure strength. However, it is noted that while  $p$ -values were very small ( $<0.001$ ) for supported area strength regardless of load type,  $p$ -values were greater for spacing when contact strength was considered, meaning height is more significant than spacing in determining the contact strength of a support structure. This is to be expected as contact strength is dependent on support structure geometry, whereas supported area strength is related to the area of the component-support structure interface.

Regression analysis was performed for both supported and contact strengths for both peel and normal loadings. Equations were generated which provide a DFAM tool for practicing engineers who intend to predict the mechanical requirements for aluminium SLM support structures (Eqs. (3)–(6)). The correlations observed for these predictive relationships vary between relatively strong ( $R^2 = 86.6\%$ ,  $\sigma_{s,peel}$ ) and relatively weak ( $R^2 = 56.6\%$ ,  $\sigma_{c,peel}$ ). The contact area strength is intended to decouple strength

characterisation from support spacing, resulting in a low correlation between these properties.

$$\sigma_{s,peel} = 64.4 - 13.3H - 13.0S + 1.28H^2 \quad (R^2 = 86.6\%) \quad (3)$$

$$\begin{aligned} \sigma_{s,normal} = & 233.7 - 39.2H - 140.7S + 3.9H^2 \\ & + 46.8S^2 \quad (R^2 = 74.1\%) \end{aligned} \quad (4)$$

$$\begin{aligned} \sigma_{c,peel} = & 121.1 - 8.9H - 66.8S + 3.08H^2 + 52.4S^2 \\ & - 16.9HS \quad (R^2 = 56.6\%) \end{aligned} \quad (5)$$

$$\begin{aligned} \sigma_{c,normal} = & 244.3 - 106.7H + 303S + 11.0H^2 \\ & - 141.1S^2 \quad (R^2 = 67.9\%) \end{aligned} \quad (6)$$

Where:

$\sigma_{s,peel}$  = Predicted supported area peel strength (MPa)

$\sigma_{s,normal}$  = Predicted supported area normal strength (MPa)

$\sigma_{c,peel}$  = Predicted contact peel strength (MPa)

$\sigma_{c,normal}$  = Predicted contact normal strength (MPa)

$H$  = Support height (mm)

$S$  = Support spacing (mm)

$R^2$  = Correlation

**Table 3**  
Numerical model parameters.

Parameter	Value
Layer thickness	0.5 mm
Platen temperature	200 °C
Powder temperature	25 °C
Volumetric energy density	$40 \times 10^9 \text{ J/m}^3$
Laser power	350 W
Material density	2780 kg/m <sup>3</sup>
Material conductivity	193 W/mK
Material specific heat	875 J/kgK

#### 4.3. Thermal FE analysis

All geometries exhibited qualitatively similar behaviour during thermal simulation (Fig. 17). During the fabrication of the solid sections of the specimen (Fig. 17 A, E), the observed temperature tends to increase linearly. A similar observation is made in the support region that is absent of teeth geometry (Fig. 17 C). However, the maximum observed temperature drops in the region of the support geometry associated with support structure teeth (Fig. 17,

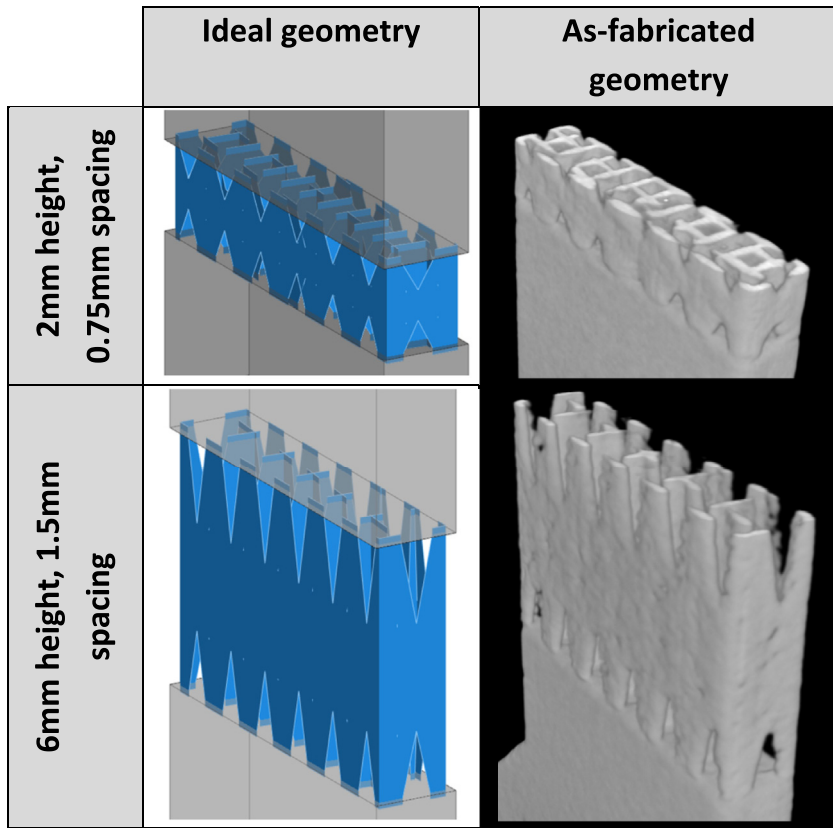


Fig. 11. Comparison of ideal and as-manufactured support structure geometries.

B,D). The explicit variation observed between the assessed geometries is presented in Fig. 18.

Specimens with the greatest height consistently experienced the greatest observed temperature. For specimens with the same height, specimens with the greatest spacing consistently experienced the greatest maximum temperature. This observation would

suggest that an increased support spacing results in an increased resistance to heat transfer, thereby increasing the maximum temperature experienced during fabrication. These observations may be influenced by the excellent thermal conductivity capacity of aluminium and may not be applicable to other less conductive metals such as titanium.

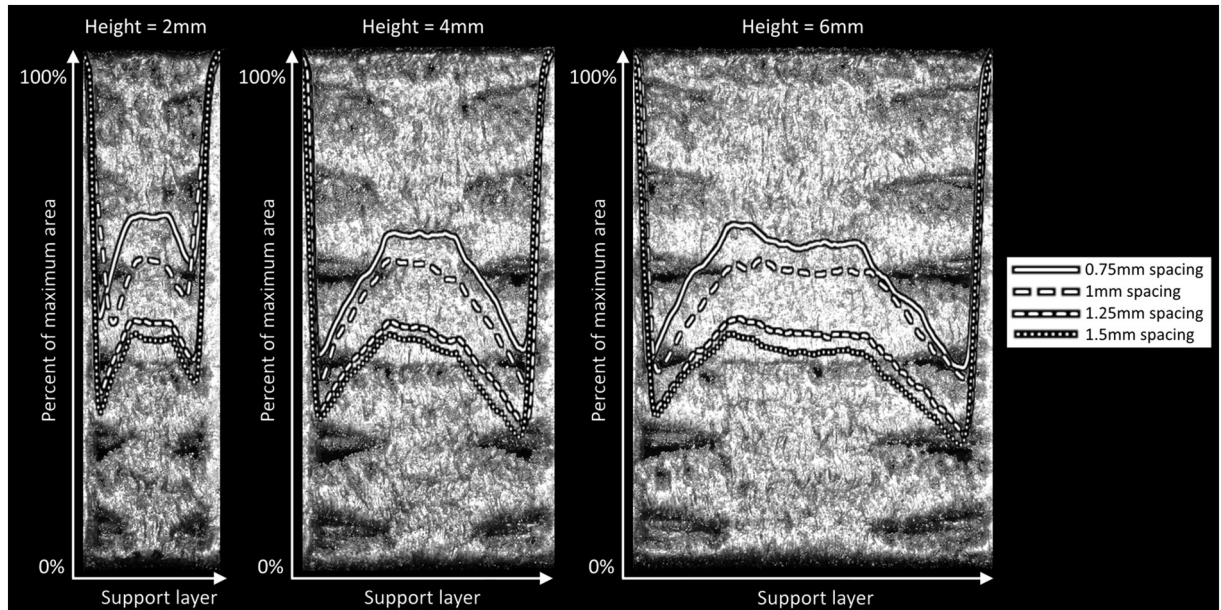
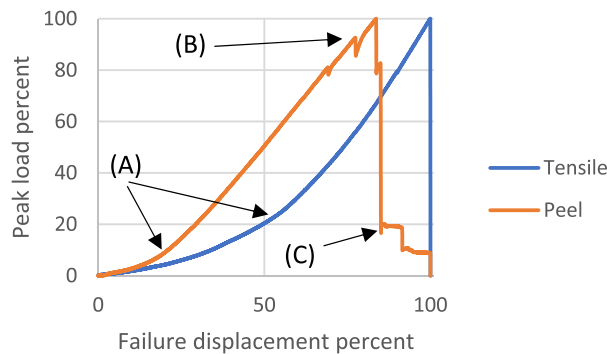


Fig. 12. Variation in cross-sectional area versus height of as-fabricated support structures. For reference, this data is superimposed on an optical microscope image of the as-fabricated support structure geometry.



**Fig. 13.** Normal and peel specimen general behaviour. An approximately linear region initiates after initial ramp up (A). Individual ligament failure is represented by dips in the curves (B) but does not lead to immediate failure of the structure. Normal specimens completely failed upon material yielding, whereas peel specimens failed progressively (C).

## 5. Discussion

Despite the criticality of robust support structure design, very little quantitative data exists to characterise their observed failure modes and mechanical response. The experimental and numerical data generated in this research assists in overcoming this critical deficiency and provides practical data relevant for design engineers, as well as insights into fundamental opportunities for support structure optimisation.

Experimental results for both mechanical testing and thermal FE demonstrate that the considered control factors – loading type, support structure spacing and height – are significant in determining the behaviour of SLM AlSi10Mg block support structures.

Support teeth geometry result in stress concentrations at the solid component-support structure interface. This stress concentration facilitates support removal, and as fracture occurs close to the component surface, net or near-net manufacture can be achieved. Taller support structures were found to have reduced minimum cross-sectional area compared to the shortest supports. This is related to the observation that the shortest support structures were found to be significantly stronger than taller support

structures. This suggests the stress-concentration effect of teeth is reduced for shorter support structures – an observation that designers should be aware of when design scenarios necessitate very short support structures.

Although support spacing was found to not affect the mechanical performance of support structures as significantly as height or loading type, thermal FE results suggest reducing spacing is a viable means of minimising component temperatures during SLM fabrication. However, this may be due to the high thermal diffusivity of aluminium, and further studies are required to identify whether this effect is material-dependent.

Comparison of supported area and contact strengths demonstrates support structure strength is highly dependent on local geometry which is not captured by supported area strength. While supported area strength is easier to assess than contact strength, these findings suggest contact strength to be a superior means of determining true support structure strength, and more useful for support structure optimisation.

Greater loads are required to fracture normally-loaded specimens than equivalent peel-loaded specimens. This variation in observed response occurs as normal loads are distributed across the entire structure, resulting in parallel load paths within all support ligaments; whereas peel loads result in stress concentrations as loads are localised within fewer ligaments, resulting in a progressive weak-link failure. This observation implies that the tensile strength of a support structure may underrepresent the mechanical response of PBF support structures, which in practice may be subject to peel loads.

This research is based on the application of best-practice commercial support design tools. A fundamental assessment of the observed failure of support structure specimens demonstrates a relationship between peak strength and support height – specifically that 2 mm support structures display a proportionately different cross-section and stress concentrating effect than those of the other assessed specimens. This observation implies that current support generation methods are sub-optimal from a practical perspective as they are functionally dependant on the associated support structure geometry. This observed deficiency can be redressed by research programs that quantify and eliminate this geometric dependency in support structure design.

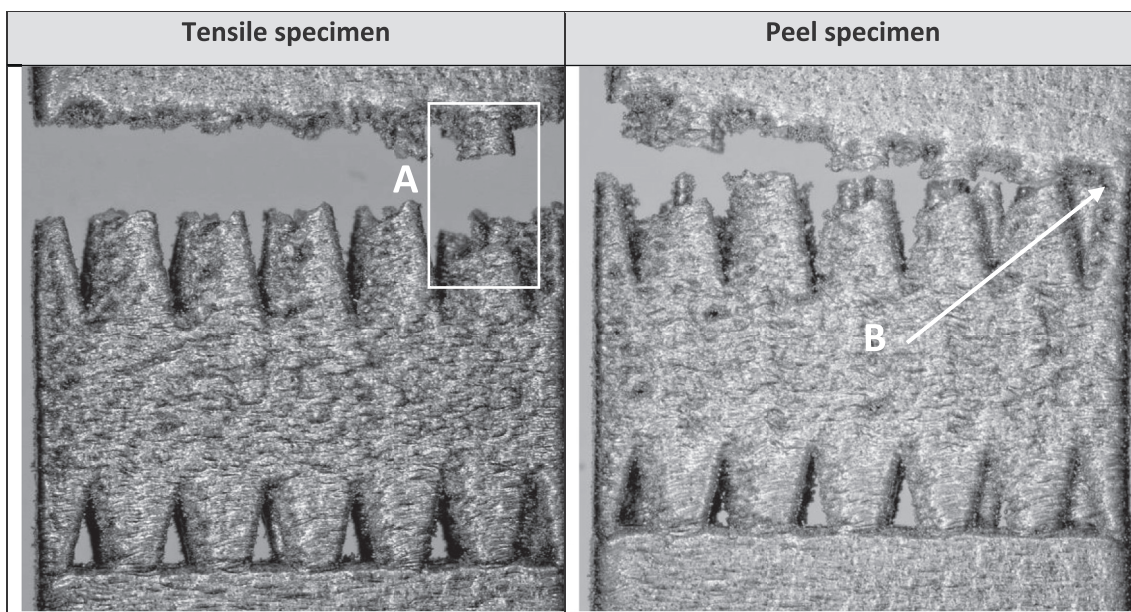


**Fig. 14.** Support-solid interface of tensile and peel specimens after failure. Normally-loaded specimen ligaments typically failed catastrophically and simultaneously, although some ligaments can be observed to have greater than average strength (A). Peel specimens fail progressively, with initial fracture on the loaded side (B).

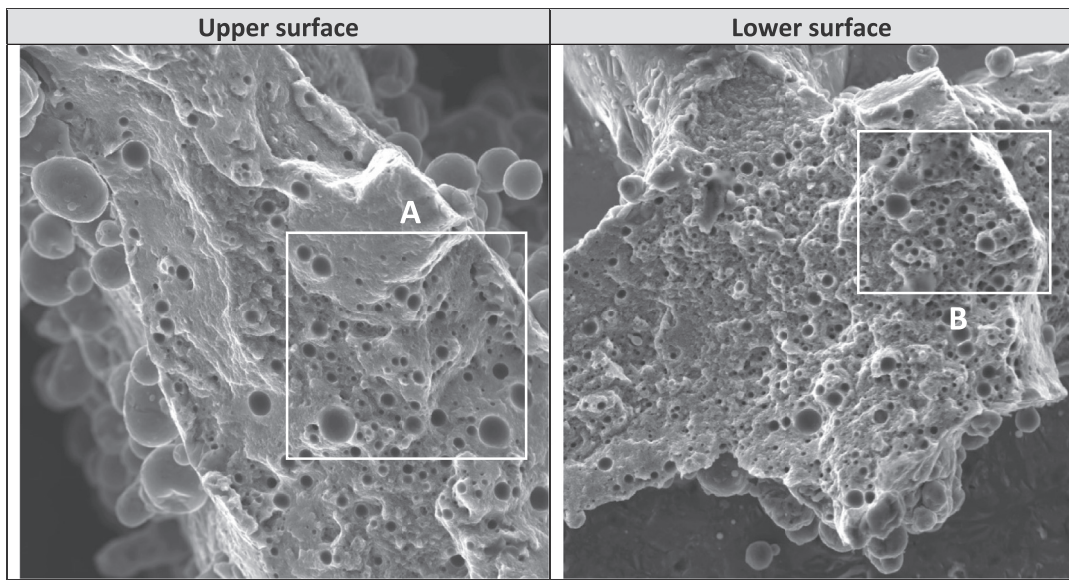


**Fig. 15.** Scanning electron microscope images of ligament fracture surfaces. Dimpled surface microstructure (A, B) suggests locally ductile fracture.

## 6. Concluding remarks

An experimental program was established in response to an identified deficiency in the understanding of the mechanical and thermal response of SLM AlSi10Mg support structures. This program

enables insight into the practical response of the associated support structures as is required to provide design engineers with pragmatic guidance for commercial applications, as well as to provide fundamental insights of benefit to research programs in support structure optimisation. Core findings of this experimental program are:

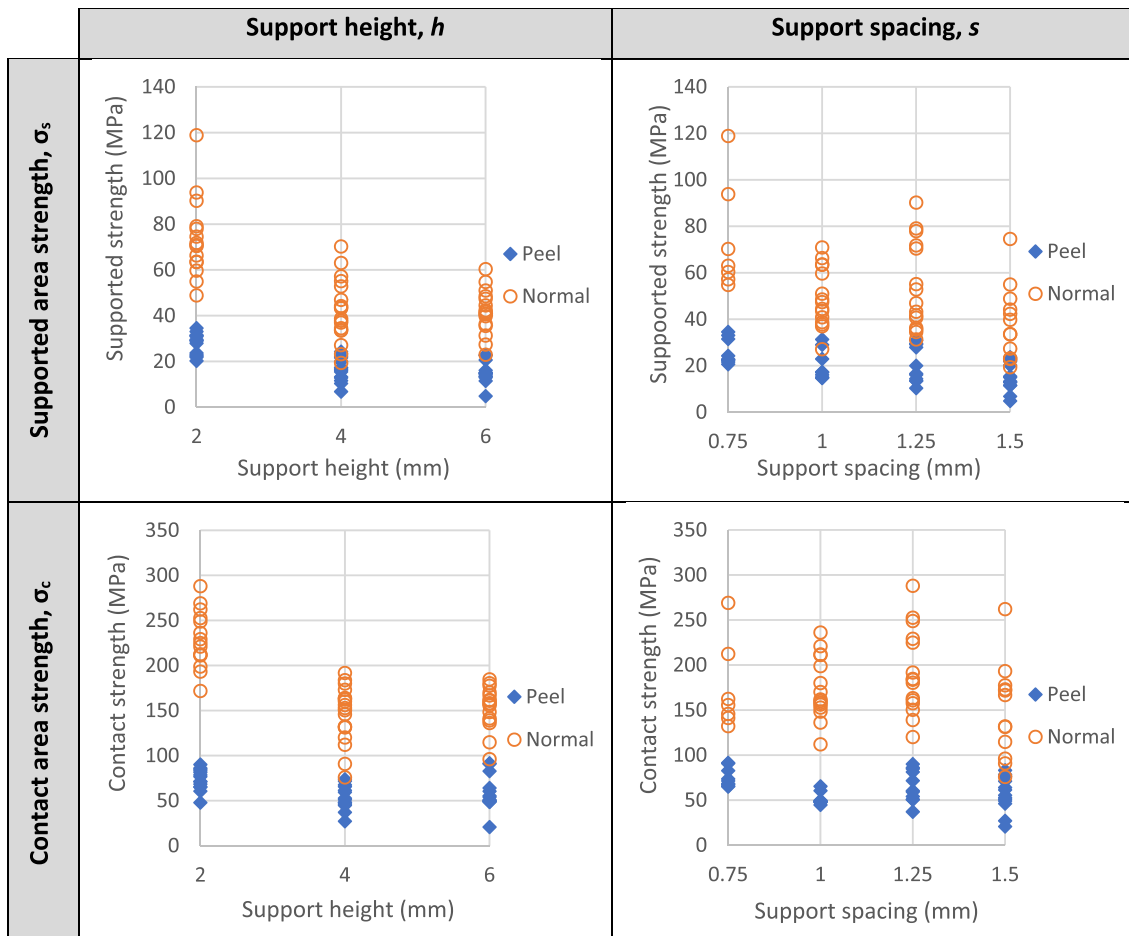


**Fig. 16.** Supported area and contact area strength compared with support structure height and spacing.

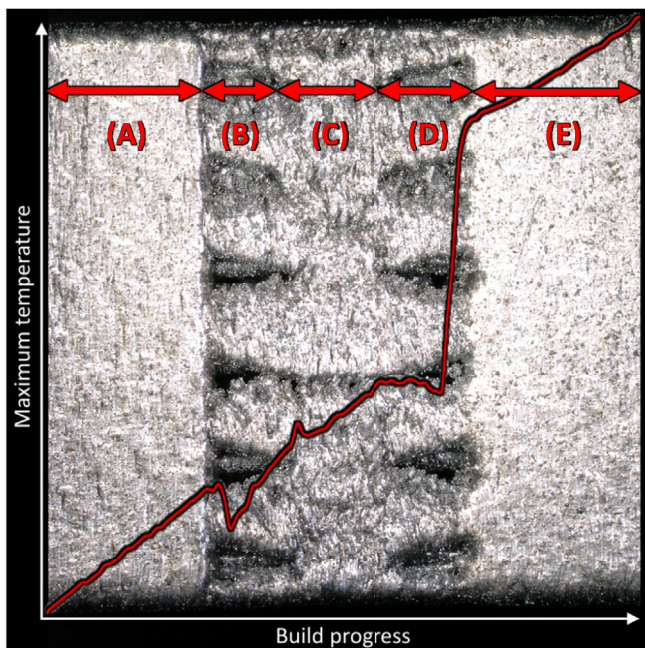


**Fig. 17.** Thermal simulation general behaviour. The build process can be broken in to five discreet stages: Lower solid section (A), lower teeth (B), central support (C), upper teeth (D) and the upper solid section (E).

- Block support structures are the most versatile of the commercially implemented support structure designs. Fundamentally different failure modes are observed for these support structures when peel and normal loads are applied.
- Normal loading results in relatively even load distributions across all support structure ligaments. These ligaments resist loading in parallel until catastrophic failure.
- Peel loading results in an uneven distribution of stress concentrated within fewer ligaments, resulting in progressive failure by a relatively weak-link failure mechanism.
- For both normal and peel loading conditions, the observed fracture is macroscopically ductile and results in catastrophic failure of the support structure. However, SEM analysis of the assessed AlSi10Mg SLM support structures suggests locally ductile failure.

- Very short support structures are significantly stronger than taller structures, due to shorter support structures having a greater minimum cross-sectional area.
- Contact area strength is largely independent of support spacing. This observation is relevant to both practical and fundamental design activities as it indicates that for a given support height contact area provides a geometrically independent measure of support strength.
- Increased support spacing as well as increased support height results in greater resistance to thermal conduction and an increase in peak temperature during fabrication. This numerically observed phenomenon for aluminium alloys can be reassessed for materials with lower conductivity such as titanium.

#### CRediT authorship contribution statement

**Martin Leary:** Conceptualization, Methodology, Resources, Writing - original draft, Writing - review & editing, Visualization, Project administration, Funding acquisition. **Tobias Maconachie:** Software, Formal analysis, Investigation, Data curation, Writing - original draft, Writing - review & editing, Visualization. **Avik Sarker:** Formal analysis, Data curation, Visualization. **Omar Farque:** Resources, Supervision, Project administration, Funding acquisition. **Milan Brandt:** Resources, Supervision, Project administration.

#### Acknowledgements

The authors would like to acknowledge the financial support from the members of the ARC Training Centre for Lightweight Automotive Structures and from the Australian Research Council (Grant Reference IC160100032).

The authors acknowledge the facilities, and the scientific and technical assistance of the RMIT Advanced Manufacturing Precinct.

#### Data availability statement

The raw/processed data required to reproduce these findings cannot be shared at this time due to technical or time limitations.

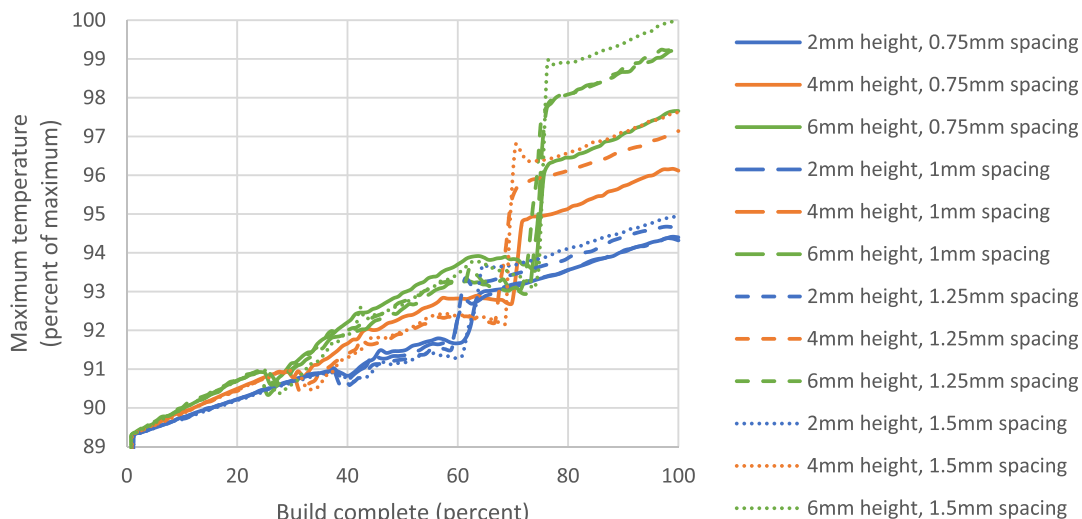


**Fig. 18.** Maximum temperature versus build percent for all observed specimens.

## Appendix 1. Analysis of variance (ANOVA)

**Table 4**

ANOVA for supported area strength subject to normal loads.

Source	Degrees of freedom	Adjusted sum of squares	Adjusted mean square	F-test statistic	P-value
Spacing	3	5380	1793.3	22.7	<0.001
Height	2	10,166	5082.8	64.33	<0.001
Error	43	3398	79		
Total	48	19,230			

**Table 5**

ANOVA for contact strength subjected to normal loads.

Source	Degrees of freedom	Adjusted sum of squares	Adjusted mean square	F-test statistic	P-value
Spacing	3	8751	2916.9	4.19	0.011
Height	2	63,302	31,651	45.4	<0.001
Error	43	29,953	696.7		
Total	48	105,578			

**Table 6**

ANOVA for supported area strength subjected to peel loads.

Source	Degrees of freedom	Adjusted sum of squares	Adjusted mean square	F-test statistic	P-value
Spacing	3	628.0	209.3	31.7	<0.001
Height	2	1331.4	665.7	100.8	<0.001
Error	36	237.7	6.603		
Total	41	2232.1			

**Table 7**

ANOVA for contact strength subjected to peel loads.

Source	Degrees of freedom	Adjusted sum of squares	Adjusted mean square	F-test statistic	P-value
Spacing	3	2996	998.8	6.23	0.002
Height	2	2862	1431.1	8.9	0.001
Error	36	5774	160.4		
Total	41	11,770			

## References

- [1] D. Appleyard, Powering up on powder technology, *Metal Powder Report* 70 (6) (2015) 285–289.
- [2] M. McMillan, et al., SLM lattice thermal fields acquired by wide-field thermal camera, *Procedia CIRP* 74 (2018) 122–126.
- [3] D. Waryoba, et al., Microtexture in additively manufactured Ti-6Al-4V fabricated using directed energy deposition, *Mater. Sci. Eng. A* 734 (2018) 149–163.
- [4] A.S. Wu, et al., An experimental investigation into additive manufacturing-induced residual stresses in 316L stainless steel, *Metall. Mater. Trans. A* 45 (13) (2014) 6260–6270.
- [5] Kleszczynski, S., et al. Improving process stability of laser beam melting systems. in: Fraunhofer Direct Digital Manufacturing Conference. 2014. Berlin, Germany.
- [6] D. Morgan, E. Agba, C. Hill, Support structure development and initial results for metal powder bed fusion additive manufacturing, *Procedia Manufacturing* 10 (2017) 819–830.
- [7] F. Calignano, Design optimization of supports for overhanging structures in aluminum and titanium alloys by selective laser melting, *Mater. Des.* 64 (2014) 203–213.
- [8] A. Hussein, et al., Advanced lattice support structures for metal additive manufacturing, *J. Mater. Process. Technol.* 213 (7) (2013) 1019–1026.
- [9] J. Jiang, X. Xu, J. Stringer, Support structures for additive manufacturing: a review, *Journal of Manufacturing and Materials Processing* 2 (4) (2018) 64.
- [10] A. Kolomiets, et al., Benefits of additive manufacturing for industrial design development. Trends, limitations and applications, *Global Journal of Research In Engineering* 18 (2-J) (2018).
- [11] L.D. Bobbio, et al., Characterization of the strength of support structures used in powder bed fusion additive manufacturing of Ti-6Al-4V, *Additive Manufacturing* 14 (2017) 60–68.
- [12] C. Brice, et al., Precipitation behavior of aluminum alloy 2139 fabricated using additive manufacturing, *Mater. Sci. Eng. A* 648 (2015) 9–14.
- [13] M. Leary, Materials selection and substitution using aluminium alloys, in: R. Lumley (Ed.), *Fundamentals of Aluminium Metallurgy: Production, Processing and Applications*, Woodhead Publishing Limited, Cambridge UK, 2011, pp. 784–827.
- [14] K.J. Maloney, et al., Multifunctional heat exchangers derived from three-dimensional micro-lattice structures, *Int. J. Heat Mass Transf.* 55 (9–10) (2012) 2486–2493.
- [15] J.R. Davis, *Aluminum and Aluminum Alloys*, ASM International, 1993.
- [16] K. Kempen, et al., Mechanical properties of AlSi10Mg produced by selective laser melting, *Phys. Procedia* 39 (2012) 439–446.
- [17] M. McMillan, M. Leary, M. Brandt, Computationally efficient finite difference method for metal additive manufacturing: a reduced-order DFAM tool applied to SLM, *Mater. Des.* 132 (2017) 226–243.
- [18] B. Vandenbroucke, J.-P. Kruth, Selective laser melting of biocompatible metals for rapid manufacturing of medical parts, *Rapid Prototyp. J.* 13 (4) (2007) 196–203.
- [19] E. Malekipour, A. Tovar, H. El-Mounayri, Heat conduction and geometry topology optimization of support structure in laser-based additive manufacturing, in: *Mechanics of Additive and Advanced Manufacturing* vol. Volume 9, Springer International Publishing, Cham, 2018.
- [20] I. Armandáriz, et al., Strategies for dynamic failure analysis on aerospace structures, in: *Handbook of Materials Failure Analysis with Case Studies from the Aerospace and Automotive Industries*, Elsevier, 2016, pp. 29–55.
- [21] M. Cloots, A.B. Spierings, K. Wegener, Assessing new support minimizing strategies for the additive manufacturing technology SLM, in: *Solid Freeform Fabrication Symposium (SFF)*, 2013 (Austin, Texas).
- [22] M. Sinnave, *Magics Print Metal User Guide*, Materialise, Belgium, 2017.
- [23] G. Strano, et al., A new approach to the design and optimisation of support structures in additive manufacturing, *Int. J. Adv. Manuf. Technol.* 66 (9–12) (2013) 1247–1254.
- [24] M.X. Gan, C.H. Wong, Practical support structures for selective laser melting, *J. Mater. Process. Technol.* 238 (2016) 474–484.
- [25] K. Zeng, Optimization of Support Structures for Selective Laser Melting, 2015.

- [26] L.J. Gibson, M.F. Ashby, *Cellular Solids: Structure and Properties*, Cambridge university press, 1999.
- [27] D. Gu, et al., Laser additive manufacturing of metallic components: materials, processes and mechanisms, *Int. Mater. Rev.* 57 (3) (2012) 133–164.
- [28] S. Clijsters, et al., In situ quality control of the selective laser melting process using a high-speed, real-time melt pool monitoring system, *Int. J. Adv. Manuf. Technol.* 75 (5) (2014) 1089–1101.
- [29] T.G. Spears, S.A. Gold, In-process sensing in selective laser melting (SLM) additive manufacturing, *Integrating Materials and Manufacturing Innovation* 5 (1) (2016) 16–40.
- [30] B. Lane, et al., in: U.S.D.o. Commerce (Ed.), *Measurement Science Needs for Real-Time Control of Additive Manufacturing Powder Bed Fusion Processes*, National Institute of Standards and Technology, 2015.
- [31] Q. Han, et al., Manufacturability of AlSi10Mg overhang structures fabricated by laser powder bed fusion, *Mater. Des.* 160 (2018) 1080–1095.